Int. J. Heat Mass Transfer. Vol. 35, No. 1, pp. 195–205, 1992
Printed in Great Britain

0017–9310/92 $5.00 + 0.00

Analysis and experiment of non-Darcian convection in horizontal square packed-sphere channels—1. Forced convection

F. C. CHOU, W. Y. LIEN† and S. H. LIN
Department of Mechanical Engineering, National Central University, Chung-Li 32054, Taiwan, Republic of China

(*Received* 10 *September* 1990 *and in final form* 28 *January* 1991)

Abstract—A numerical and experimental investigation of non-Darcian forced convection in horizontal square packed-sphere channels is presented. The theoretical results are found to be in agreement with the experimental results. The values of the fully-developed Nusselt number are influenced mainly by the channelling effect when the Peclet number is small, but the thermal dispersion effect becomes dominant when the Peclet number is high. The effect of thermal dispersion on heat transfer is rather weak in the near entrance region but becomes relatively significant in the thermally fully-developed region. The ratio of equivalent hydraulic diameter to sphere diameter, D_e/d, significantly affects the Nusselt numbers when the Peclet number is high; it is caused again mainly by the thermal dispersion effect.

1. INTRODUCTION

THE STUDY of convective heat transfer in a porous medium has been the subject of many recent studies due to the increasing need for better understanding of the associated transport processes in packed-sphere beds, geothermal systems, thermal insulations, grain and coal storage, solid matrix heat exchangers, and oil extraction. The majority of the existing studies pertaining to heat and fluid flow in a porous medium make use of the Darcy flow model. One of the first theoretical attempts to account for boundary and inertial effects in forced convective flow through a porous medium confined by an isothermal plate was carried out by Vafai and Tien [1]. Vafai [2] and Vafai *et al.* [3] studied theoretically and experimentally the channelling effect on the forced convection along an isothermal flat plate. Kaviany [4] studied a laminar flow through a porous medium bounded by isothermal parallel plates with the Brinkman-extended flow model and constant matrix porosity. Cheng and Hsu [5] analysed the wall effect on the thermal dispersion process in the forced convective flow through an annular packed-sphere bed. Effects of radial thermal dispersion on fully-developed forced convection in cylindrical packed tubes was studied by Cheng and Zhu [6]. Later, Cheng and Vortmeyer [7] studied the effect of transverse thermal dispersion on fully-developed forced convection in a packed bed bounded between parallel plates. Theoretical and experimental studies on forced convection in an isothermal channel with the effects of inertia, variable porosity and Brinkman friction taken into account were reported by Poulikakos and Renken [8] and Renken and Poulikakos [9, 10]. Non-Darcian forced convection in cylindrical packed beds, including the effects of flow inertia, channelling, solid-boundary shear and thermal dispersion was studied theoretically by Hunt and Tien [11]. Kuo and Tien [12] used the mixing-length concept and statistical averaging to depict the transverse dispersion process in packed-sphere beds. Beckermann and Viskanta [13] and Nakayama *et al.* [14] presented analytical solutions to the problem of forced convection along a flat plate in a porous medium by including the effects of inertia and boundary. Non-Darcian forced convection in a parallel plate channel filled with packed spheres was studied in ref. [15].

Though experiments were conducted in rectangular channels with aspect ratios (width/height) of about 4 [3] and 2 [9, 10], the corresponding theoretical models were for flow along a flat plate [3, 10] or in a parallel plate channel [9]. The above brief survey of the literature reveals that a theoretical and experimental study on non-Darcian forced convection in square channels filled with packed spheres is nonexistent. Furthermore, as shown in Fig. 1, the theoretical predictions of Nusselt number for a square channel by using the existing theoretical non-Darcian forced convection models, which were for a parallel plates channel [8, 12] or cylindrical packed beds [6, 11], are not consistent. The aim of the present paper is to study theoretically and experimentally the non-Darcian forced convection in packed-sphere square channels with the consideration of the flow inertia, boundary, channelling and thermal dispersion effects. The present results can provide a basis to study the non-Darcian mixed convection in the second part of this subject.

† Present address: Power Mechanical Engineering Department, Tsing-Hua University, Hsin-chu, Taiwan, Republic of China.

NOMENCLATURE

A	cross-sectional area
a	width of rectangular channel
a_1, a_2	coefficients used in porosity variation, equation (5)
a_3	thermal dispersion damping constant, equation (12)
b	height of rectangular channel
C	inertia coefficient, equation (7)
c_p	specific heat at constant pressure
d	particle diameter
D	diameter of the packed beds in Benenati and Brosilow [16]
Da	Darcian number, K_∞/d^2
D_e	equivalent hydraulic diameter, $4A/S$
$\bar{h}$	heat transfer coefficient
K	permeability
K_P	wall conduction parameter, equation (10), $k_w t/(k_f d)$
k	thermal conductivity
l	mixing length, equation (8)
M, N	number of divisions in the X- and Y-directions
Nu	Nusselt number, $\bar{h}D_e/k_f$
n	inward normal
n^*	dimensionless inward normal, equation (10), n/d
p	pressure
Pe	Peclet number, $Pr\,Re$
Pr	Prandtl number, ν_f/α_f
q_w	prescribed uniform heat flux on the outside surface of the channel wall
Re	Reynolds numbers based on the sphere diameter, $\langle\bar{w}\rangle d/\nu_f$
S	circumference of cross-section
s^*	dimensionless quantity of S, equation (10), S/d
T	temperature
t	thickness of channel wall
W	dimensionless axial velocity
$\langle\bar{w}\rangle$	cross-sectional averaged axial fluid velocity
X, Y, Z	dimensionless rectangular coordinates
x, y, z	rectangular coordinates.

Greek symbols

α	thermal diffusivity
γ	coefficient in dispersion conductivity, equation (8)
ε	porosity
θ	dimensionless temperature
μ	dynamic viscosity
ν	kinematic viscosity
ρ	density.

Subscripts

b	bulk mean temperature
c	characteristic quantity
d	dispersion
e	effective
f	fluid
o	stagnant
ref	reference quantity
w	wall
∞	quantity in the core region
Γ	inside surface of the channel wall.

2. EXPERIMENTAL APPARATUS AND PROCEDURES

The experimental apparatus is shown in Fig. 2. The heated test section is preceded by a constant head tank with an overflow bypass for water head control and a 10 cm long channel for flow development before entering the test section, since the hydraulic entrance region is important only for a distance of $O(Kw/\nu_f)$ [1], where K is the permeability of the porous medium, w the axial fluid velocity, and ν_f the kinematic viscosity of the fluid. The heated sections were made of 4.75×4.75 cm stainless steel square channel of length 65 cm and 9.5×9.5 cm aluminium square channel of length 40 cm with 2 mm thick walls. The square channels are packed with 5 mm diameter glass spheres. The experiments in the two channels are described as cases 1 and 2 in Table 1. Special care was taken in packing the beads to ensure uniformity in the structure of the porous medium. The spheres were poured randomly into the channel, levelled and then shook. This procedure was repeated until no more beads could be placed into the channel. Two stainless steel screens are placed at the inlet and outlet of the channel to hold the beads in place. The measured global porosity for the whole packed-sphere channel is 0.365 for the stainless steel channel and 0.35 for the aluminium channel. It was shown in the results of Benenati and Brosilow [16] that for uniform spheres, the average porosity for $D/d = 14.1$ is slightly higher than that for $D/d = 20.3$, where D and d are the diameters of bed and ball, respectively. In a similar way, the present results that the average porosity for $D_e/d = 10$ is slightly higher than that for $D_e/d = 19$ is reasonable, where D_e is the equivalent hydraulic diameter. Electric power from four auto-transformers provided Joulean heating for four main heaters on four channel walls. Guard heaters were placed outside of the main heaters to prevent heat loss from the main heaters to the surroundings. The inlet fluid bulk temperature was measured in the fluid at the centre of the inlet of the channel. The volumetric flow rate was measured by

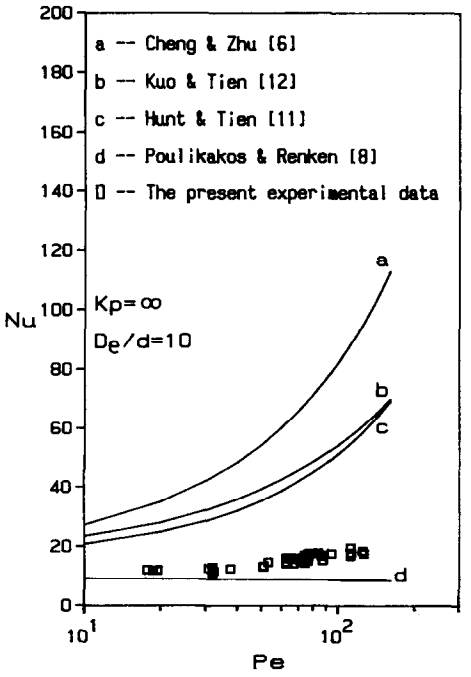

IG. 1. Comparison of the theoretical predictions of Nusselt number by the existing models.

using a measuring glass and a stop watch. Then the cross-sectional averaged axial fluid velocity, $\langle \bar{w} \rangle$, and Reynolds number, $Re = \langle \bar{w} \rangle d/\nu_f$, were obtained.

The value of the average heat input to the fluid was required in the calculation of the heat transfer coefficient. The power for each heater was measured with a digital multimeter and a standard shunt resistor. Each main heater was adjusted to give equal power. The value of the averaged heat flux is determined by the total power dissipation and the heated area. The variation of wall temperature was measured by nine copper–constantan T type thermocouples at a cross-section. These nine thermocouples were arranged circumferentially as shown in Fig. 2(b). The averaged wall temperature was calculated by averaging the readings of the nine copper–constantan thermocouples which are placed at an axial position located 45 and 35 cm from the entrance of the heated section in cases 1 and 2, respectively. Prior to installation the thermocouples were calibrated using an ice bath. The overall accuracy was found to be within $\pm 0.1°C$.

Water was chosen as the working fluid because of its availability and wide application. The test generally proceeded by maintaining the flow rate, input power

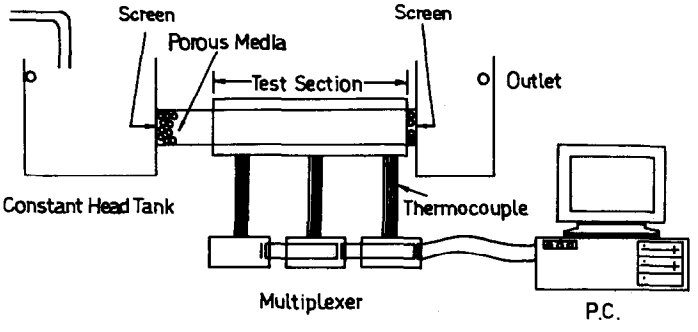

(a)

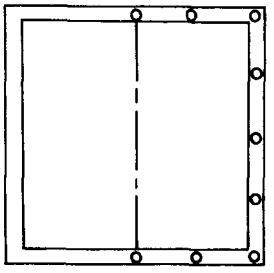

(b)

FIG. 2. (a) Experimental apparatus. (b) Schematic of thermocouple set-up.

Table 1. Brief description of the experiments: cases 1 and 2

	Case 1	Case 2
Dimension of channel	4.75 × 4.75 × 85 cm	9.5 × 9.5 × 60 cm
Materials of channel	stainless steel	aluminium
Length for hydraulic development	10 cm	10 cm
Length of heated section	65 cm	65 cm
Average porosity, $\bar{\varepsilon}$	0.365	0.35

and inlet fluid temperature fixed. After a steady state was reached, the variation of wall temperatures was recorded. It is sufficient to determine the average wall temperature with nine temperature readings for the half circumference under the condition of symmetry. The data of flow rate, inlet fluid temperature, and electric power input were also recorded. The local bulk mean temperature of the fluid at the measuring section was calculated from the values of the inlet temperature, flow rate and power input. The fluid enthalpy rise could be used as a double check to the electric power inputs by measuring the bulk fluid temperature in the mixing chamber. The experimental error in heat balance was found to be less than 4%. The average wall temperature was calculated using Simpson's rule for the measured data of nine thermocouples at a cross-section. The nine thermocouples are connected through a multiplexer to a personal computer. The local heat transfer coefficient $\bar{h}$ was calculated by the local heat flux, averaged wall temperature and the local bulk mean fluid temperature. The evaluation of Nusselt number is based on the equivalent hydraulic diameter D_e and the fluid conductivity k_f as follows:

$$Nu = \bar{h}D_e/k = q_w D_e/[k_f(\bar{T}_w - T_b)] \quad (1)$$

where q_w is the heat flux imposed at the outer surface of channel walls, and $\bar{T}_w$ and T_b are the averaged wall temperature and bulk mean fluid temperature. All of the fluid properties (density, specific heat, dynamic viscosity and thermal conductivity) were evaluated at the local film temperature which is the arithmetic mean of the local bulk mean fluid temperature and averaged wall temperature.

The procedure to collect experimental data was repeated rigorously for each test run. A steady state condition was said to be reached when the deviations of wall temperature and local bulk fluid temperature are all within ± 0.1°C for 30 min. After each test run the channel was emptied, flushed and refilled with water. In all the experiments, the difference of average wall-to-fluid bulk mean temperature was maintained within 4–6°C in order to reduce the non-constant property effects. Thus the buoyancy effect on the forced convective flow can be neglected. The experimental uncertainties in Nusselt number mainly due to experimental errors in heat balance and temperature measurements are estimated to be in the range from 11 to 16%. The larger uncertainties are due to smaller temperature difference $(\bar{T}_w - T_b)$.

3. NUMERICAL SIMULATIONS

A schematic of the problem used for numerical simulation of non-Darcian forced convection in a horizontal square channel filled with packed spheres is shown in Fig. 3. A steady fully developed velocity profile is assumed at the entrance of the heated section and a uniform wall heat flux, q_w, is imposed on each outer surface of the channel wall. Referring to the coordinate system shown in Fig. 3, the following dimensionless variables and parameters are introduced:

$$X = x/d, \quad Y = y/d, \quad Z = z/(d\,Pe), \quad W = \langle w\rangle/\langle \bar{w}\rangle$$

$$\theta = (\langle T\rangle - \langle T_{ref}\rangle)/\theta_c, \quad \theta_c = q_w d/k_f, \quad Da = K_x/d^2$$

$$Re = \langle \bar{w}\rangle d/\nu_f, \quad Pr = \nu_f/\alpha_f, \quad Pe = Pr\,Re. \quad (2)$$

The following governing equations can be obtained:

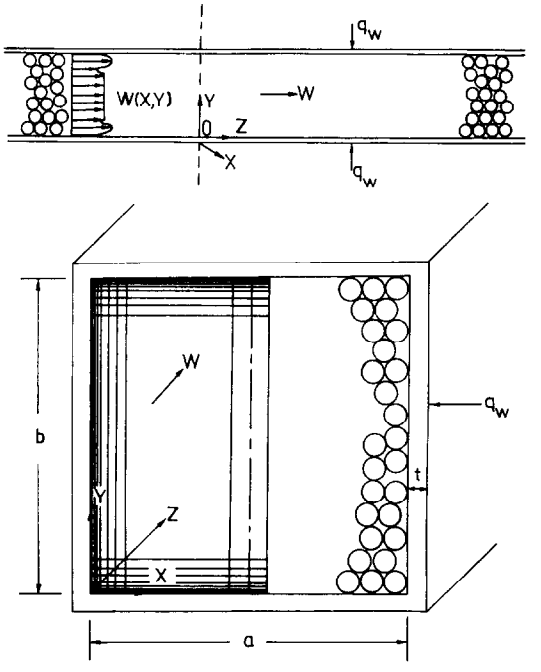

FIG. 3. Schematic for the numerical solution and the coordinate system.

$$0 = \varepsilon[-K_\infty(\mathrm{d}p/\mathrm{d}z)/(\mu\langle\bar{w}\rangle)]/Da-(\varepsilon d^2/K)W - \varepsilon C d\, Re\, W^2+\partial^2 W/\partial X^2+\partial^2 W/\partial Y^2 \quad (3)$$

$$W\partial\theta/\partial Z = (\partial/\partial X)[(k_e/k_f)(\partial\theta/\partial X)] + (\partial/\partial Y)[(k_e/k_f)(\partial\theta/\partial Y)] + (\partial/\partial Z)[(k_e/k_f)(\partial\theta/\partial Z)]/Pe^2 \quad (4)$$

where d is the diameter of the packed sphere, $\langle\ \rangle$ represents a volume-averaged quantity, w is the local axial velocity, Da the Darcian number, ε the porosity, K and C are the permeability and inertial coefficient, the subscript ∞ represents a quantity in the core region, and k_e and k_f are the effective and fluid conductivity. The inlet fluid temperature and the wall temperature at the corner are taken as the reference temperature, T_{ref}, for the thermal entrance and fully-developed problems, respectively. The value of the dimensionless axial pressure gradient term in equation (3) is determined by the constraint $\bar{W} = 1$. The axial diffusion term vanishes when the flow is considered as thermally fully-developed. If the thermal entrance problem is considered, the axial diffusion effect is neglected by using the high Peclet number assumption as used in refs. [5–8, 11–13].

From the experimental results of Benenati and Brosilow [16], the functional dependence of the porosity ε on the distance from the channel wall can be represented approximately by an exponential function as used in refs. [2, 3, 5–12]

$$\varepsilon = \varepsilon_\infty[1+a_1\exp(-a_2 n/d)] \quad (5)$$

where ε_∞ is the porosity at the core region, n the normal distance from the wall, and a_1 and a_2 are empirical constants which depend on the ratio of the bed to particle diameter. The result of equation (5) neglects the small spatial variations of the porosity. The permeability, K, and empirical inertia coefficient, C, are given by the approximation developed by Ergun [17] for flow in a packed bed

$$K = d^2\varepsilon^3/(150(1-\varepsilon)^2) \quad (6)$$

$$C = 1.75(1-\varepsilon)/(d\varepsilon^3). \quad (7)$$

Since the porosity varies, the values of K and C vary with distance from the wall also. The effective conductivity k_e is composed of a sum of the stagnant and dispersion conductivities, $k_e = k_o + k_d$. The stagnant conductivity depends on the porosity variation and the conductivities of the fluid and solid. Since the thermal conduction of water is very close to the thermal conduction of glass spheres, $k_o/k_f = 1$ was used in the present work. It has been shown [9] that neglecting the variation of stagnant conductivity for water and glass spheres works well. The effective conductivity also includes thermal transport due to the effect of thermal dispersion. Thermal dispersion results from the existence of the solid matrix which forces the flow to undergo a tortuous path around the solid particles. The value of the thermal dispersion conductivity is proposed to be proportional to a product of the local velocity and mixing length $l(n)$ as used in refs. [6, 11, 12]

$$k_d = \gamma_\infty \rho c_p|\langle w\rangle|l(n) = k_f\gamma_\infty\, Pe\, W l(n)/d \quad (8)$$

where γ_∞ is the value of the thermal dispersion coefficient at the core region.

Because of symmetry, it suffices to solve the problem in half the rectangular region such as that shown in Fig. 3. The boundary conditions are:

$$W = 0 \quad \text{at walls}$$

$$\partial W/\partial X = \partial\theta/\partial X = 0 \quad \text{at symmetry plane } (x = a/2)$$

$$\theta = 0 \quad \text{at entrance } z = 0 \quad (9)$$

the derivation of the thermal boundary condition along the channel wall can be found in Shah and London [18] and rewritten as

$$1+(\partial\theta/\partial n^*)_\Gamma + K_P(\partial^2\theta/\partial s^{*2})_\Gamma = 0 \quad (10)$$

where condition Γ denotes the inside surface of the channel wall, $n^* = n/d$ the dimensionless inside normal, $s^* = s/d$ the dimensionless circumference of the cross-section, and $K_P = k_w t/(k_f d)$ a parameter indicating the relative importance of heat conduction along the channel wall and in the fluid. Two limiting cases, $K_P = 0$ and ∞, yield the circumferential boundary conditions of uniform heat flux and uniform wall temperature, respectively.

Since the present study pertains to forced convection, the dimensionless momentum and energy equations are decoupled, equation (3) can be solved independently to yield the velocity field. With the result of velocity in hand, the temperature field can be obtained from equation (4). After the developing fields along the axial direction are obtained, the local Nusselt number Nu can be calculated based on the overall energy balance for an axial length $\mathrm{d}z$ as

$$Nu = \bar{h}D_e/k_f = (D_e/d)/(\bar{\theta}_w - \theta_b) \quad (11)$$

where $D_e = 4A/S$ is the equivalent hydraulic diameter.

4. RESULTS AND DISCUSSION

To track accurately the developing temperature profile near the entrance and the porosity variation and the dispersion damping near the wall, a non-uniform grid system in the axial ($\Delta Z_k = 1.01\Delta Z_{k-1}$) and peripheral ($\Delta X_i = 1.05\Delta X_{i-1}$, $\Delta Y_j = 1.05\Delta Y_{j-1}$) directions is used. The numerical results should be independent of the number of non-uniform grids used. Therefore, a numerical experiment was made and the results are shown in Table 2 for the cases of $D_e/d = 10$, $Pr = 6.5$ and $Pe = 10$, 20 and 100 for both $K_P = \infty$ and 0. It is seen that the deviations of computed Nu with $M \times N = 30 \times 60$, 36×72 and 40×80 are all less than 2%. Thus $M \times N = 30 \times 60$ was used throughout the work for $D_e/d = 10$.

In obtaining the numerical results the following input parameters were used: Peclet number, Prandtl number, ratio of the equivalent hydraulic diameter to

Table 2. Numerical experiments on the non-uniform grid system $M \times N$ for the cases of $D_e/d = 10$, $Pe = 10$, 20 and 100, and $K_P = \infty$ and 0

Pe	$M \times N$	Nu
	(a) $K_P = \infty$	
	30×60	9.281
10	36×72	9.368
	40×80	9.399
	30×60	10.938
20	36×72	11.037
	40×80	10.998
	30×60	19.308
100	36×72	19.491
	40×80	19.577
	(b) $K_P = 0$	
	30×60	7.873
10	36×72	7.927
	40×80	7.951
	30×60	9.264
20	36×72	9.354
	40×80	9.342
	30×60	16.588
100	36×72	16.865
	40×80	16.925

the particle diameter D_e/d, porosity at the core region and the semi-empirical coefficients a_1 and a_2 for the porosity variation. The value of the Prandtl number is assigned as 6.5 throughout the work for water used as working fluid in the present experimental study.

Using the theoretical models established in refs. [6, 8, 11, 12], the theoretical predictions of the Nusselt number vs Peclet number in the thermally fully-developed region of a horizontal square packed-sphere channel with $D_e/d = 10$ are shown in Fig. 1. The experimental data for case 1 are also shown in Fig. 1 for comparison. The thermal boundary condition is considered as constant axial heat input and peripherally uniform wall temperature ($K_P = \infty$) for the numerical calculations. It is seen that there are quite large discrepancies among the theoretical predictions of the Nusselt number. The differences of the theoretical models used in refs. [6, 8, 11, 12] are the models of porosity variation and thermal dispersion conductivity.

Porosity: $\varepsilon = \varepsilon_\infty[1 + a_1 \exp(-a_2 n/d)]$, $\bar{\varepsilon} = 0.365$

(1) Cheng and Zhu [6]:

$$a_1 = 1, \quad a_2 = 2, \quad \varepsilon_\infty = 0.315.$$

(2) Poulikakos and Renken [8]:

$$a_1 = 0.43, \quad a_2 = 3, \quad \varepsilon_\infty = 0.352.$$

(3) Hunt and Tien [11]:

$$a_1 = 1/\varepsilon_\infty - 1, \quad a_2 = 6, \quad \varepsilon_\infty = 0.333.$$

(4) Kuo and Tien [12]:

$$a_1 = 1/\varepsilon_\infty - 1, \quad a_2 = 6, \quad \varepsilon_\infty = 0.333.$$

Thermal dispersion conductivity:

$$k_d = k_f \gamma_\infty \, Pe \, Wl(n)/d$$

(1) Cheng and Zhu [6]:

$$\gamma_\infty = 0.17, \quad l(n)/d = 1 - \exp[-n/(\delta d)], \quad \delta = 1.5.$$

(2) Poulikakos and Renken [8]:

$$k_d = 0, \text{ no dispersion.}$$

(3) Hunt and Tien [11]:

$$\gamma_\infty = 0.1, \quad l(n)/d = n/2d.$$

(4) Kuo and Tien [12]:

$$\gamma_\infty = 0.07, \quad l(n)/d = 1 - \exp[-a_3(n/d)], \quad a_3 = 5. \tag{12}$$

It can be seen from Fig. 1 that the theoretical models a, b and c overpredict the Nusselt numbers when compared with the present experimental results, while model d, which attributes to the neglect of the effect of thermal dispersion, underpredicts. The reason why theoretical models a–c overpredict is proposed as: the models of porosity and thermal dispersion conductivity in refs. [6, 11, 12] were used for circular pipes or parallel plates; however, the experimental apparatus of the present study is constructed of a horizontal square channel, thus the effects of channelling and thermal dispersion would be suppressed due to the presence of the 90° corners and the peripheral walls. Therefore, it is expected that the models of porosity variation and thermal transport due to the thermal dispersion effect especially the near-wall damping need reconsideration.

The results of Benenati and Brosilow [16] showed that the porosity falls to a minimum value at a distance of approximately half ball diameter away from the wall and oscillates through several maxima and minima before settling down to the free-stream value. In order to reflect more realistically the porosity variation, a decaying-cosine porosity is used as mentioned in Hunt and Tien [11]

$$\varepsilon = \varepsilon_\infty[1 + a_1 \exp(-a_2 n/d) \cos(2\pi n/d)]. \tag{13}$$

The empirical constants in equation (13) are chosen as $a_1 = 0.43$ and $a_2 = 3$ as used in Renken and Poulikakos [9], because the rectangular channel with aspect ratio 2 used by Renken and Poulikakos [9] is quite similar to the square channel used in the present study. The velocity profiles obtained by using the porosity variation equation (13) are shown in Fig. 4 for the cases of $Pe = 100$ and $D_e/d = 10$ and 19. This decaying oscillatory behaviour in velocity profile is qualitatively in agreement with the results of Vortmeyer and Schuster [19]. It is seen that the velocity maxima due to the channelling effect appears within half ball diameter from the wall, and the near wall velocity for $D_e/d = 10$ is higher due to the relatively stronger channelling effect rather than that of $D_e/d = 19$. Since the average values of the axial velocity for both $D_e/d = 10$ and 19 are the same under a

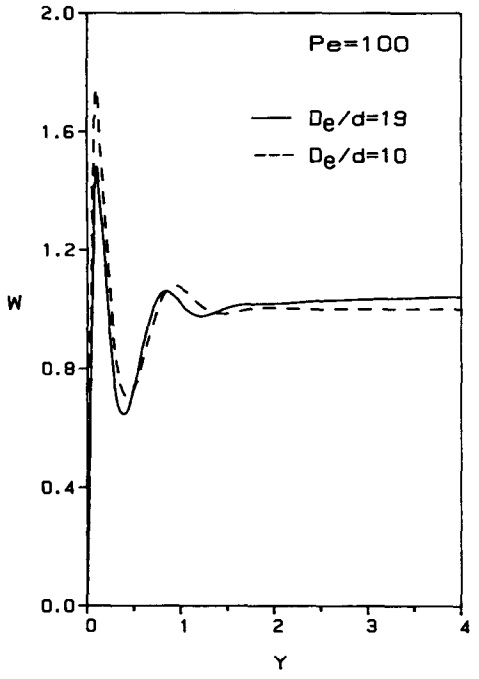

FIG. 4. Wall channelling effect on axial velocity distribution for $Pe = 100$ and $D_c/d = 10$ and 19.

fixed Pe, the core region velocity for $D_c/d = 19$ in turn is higher than that of $D_c/d = 10$.

By using the above porosity variation equation (13) and the thermal dispersion model used by Kuo and Tien [12], the present theoretical prediction and experimental data of fully-developed Nusselt number vs Peclet number are shown in Fig. 5 for thermal boundary conditions of $K_P = \infty$ and 0. The value of the thermal dispersion damping constant a_3 is determined by fitting with the experimental data. It is apparent from Fig. 5 that there is a good agreement between the experimental and the theoretical results for $a_3 = 1$. A smaller dispersion damping with $a_3 = 5$ was used by Kuo and Tien [12] for the flow along a flat plate. Since the damping of dispersion is stronger in the square channel due to the presence of four 90° corners and peripheral walls, the present model of thermal dispersion conductivity with a larger damping $a_3 = 1$ is reasonable. Perhaps it is the strong near-wall damping of thermal dispersion, which occurs also in the rectangular channel with aspect ratio 2 used by Renken and Poulikakos [9], makes the theoretical results in agreement with the experimental results, though the thermal dispersion effect was not included in their theoretical model. Then, the next necessary step is to find out whether the present theoretical model can be applied to predict the Nusselt number for the forced convection in another different size square channel. It is shown in Fig. 6 that the agreement between theoretical results and experimental data for case 2 shown in Table 1 is good overall, worse when the Peclet number is high.

Considering the flow in a square channel without packed spheres, the fully-developed Nusselt number is a unique constant and independent of fluid properties, flow velocity and size of the channel. But from a comparison between the results shown in Figs. 5 and 6, it is noteworthy that the Nusselt numbers depend not only on the value of Pe due to the thermal dis-

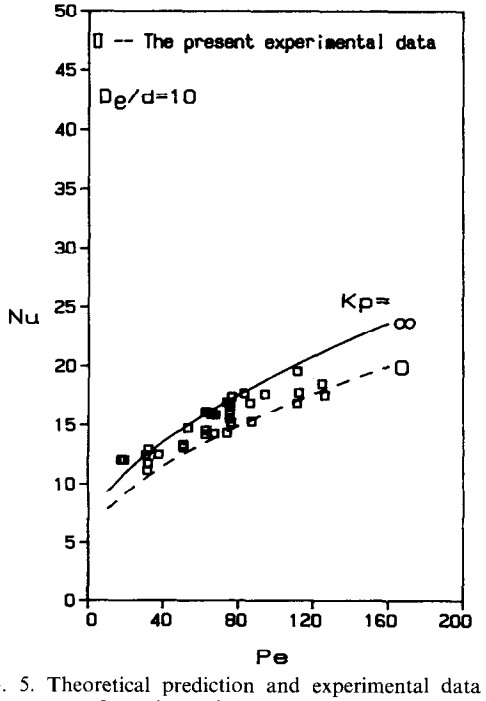

FIG. 5. Theoretical prediction and experimental data of Nusselt number for $D_c/d = 10$.

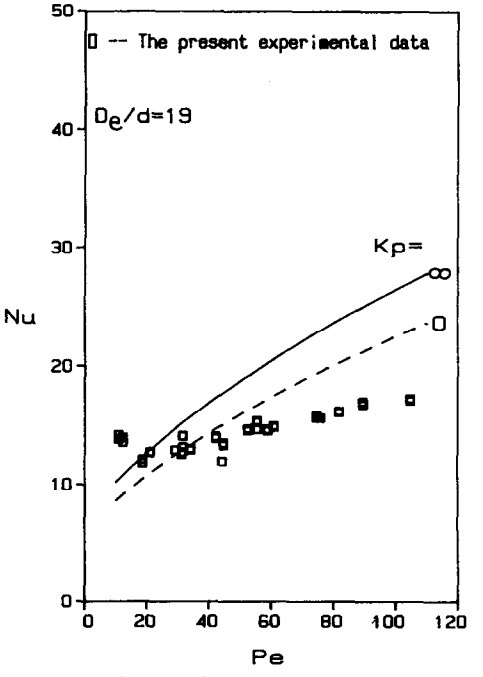

FIG. 6. Theoretical prediction and experimental data of Nusselt number for $D_c/d = 19$.

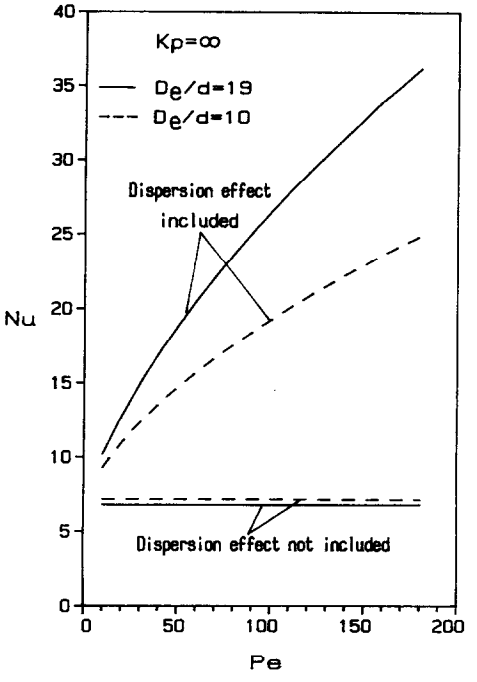

FIG. 7. Theoretical prediction of Nusselt number with thermal dispersion effect not included and included for $D_e/d = 10$ and 19.

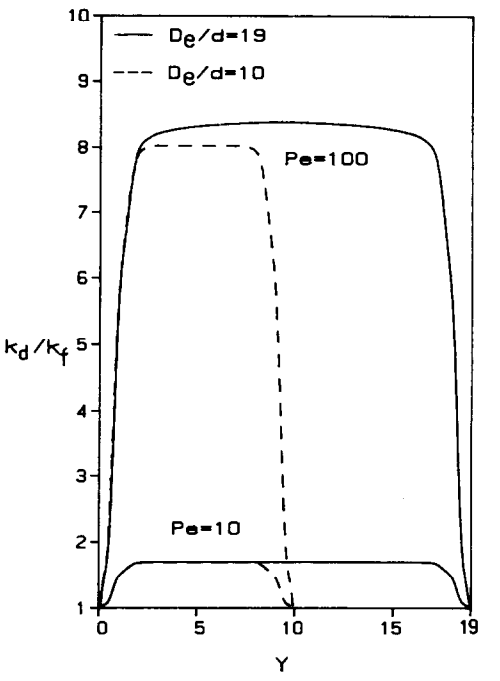

FIG. 8. Thermal dispersion conductivity distribution along the symmetrical line $x = a/2$ for $D_e/d = 10$ and 19.

persion effect but also the value of D_e/d. We need to know why and how the ratio of equivalent hydraulic diameter to the diameter of spheres D_e/d affects the Nusselt number. It is shown in Fig. 7 that the Nusselt number for $D_e/d = 10$ is slightly higher than that of $D_e/d = 19$ if the thermal dispersion effect is not included in the theoretical model. It is mainly due to the higher near-wall velocity for $D_e/d = 10$ as shown in Fig. 4. However, if the thermal dispersion effect is included, the Nusselt number for $D_e/d = 19$ becomes higher and the difference between the Nusselt number for $D_e/d = 19$ and 10 increases with the increase of Pe. In other words, even under a fixed Pe, the thermal dispersion effect will affect significantly the Nusselt numbers in the square channel with different D_e/d. For detailed inspection, the distribution of thermal dispersion conductivity k_d/k_f in the square channel with $D_e/d = 10$ and 19 is shown in Fig. 8 for the cases of $Pe = 10$ and 100. It is seen that both the values of k_d/k_f in the near wall and core region are almost the same when $Pe = 10$ for $D_e/d = 10$ and 19, but when $Pe = 100$ the values of k_d/k_f for $D_e/d = 19$ are higher than that for $D_e/d = 10$ in the core region. Though the velocity in the core region for $D_e/d = 19$ is only slightly higher than that for $D_e/d = 10$ as shown in Fig. 4, the high Peclet number such as $Pe \geqslant 100$ will magnify the difference and induce significantly higher thermal dispersion conductivity.

The dimensionless temperature distributions along the symmetrical line for the cases of $K_p = \infty$, $Pe = 10$ and 100 and $D_e/d = 10$ and 19 are shown in Fig. 9. Since the values of k_d/k_f for $Pe = 10$ and 100 are almost the same at the near-wall region, as shown in Fig. 8, the temperature distributions at the near-wall region are seen to almost coincide in Fig. 9 for $Pe = 10$ and 100 in both channels $D_e/d = 10$ and 19. But the relatively stronger thermal dispersion effect at $Pe = 100$ makes the temperature distribution in the core region much smoother than that at $Pe = 10$, and the difference between the temperature distributions of $Pe = 10$ and 100 due to the effect of thermal dispersion is larger in the channel of $D_e/d = 19$ rather than that in the channel of $D_e/d = 10$.

Figure 10 shows the variation of the Nusselt number along the thermal entry region for a wide range of Pe. It is noteworthy that the effect of Peclet number on the Nusselt number is relatively weak in the near entrance region of a channel; however, with an increase in the axial distance this effect eventually becomes significant in the thermally fully-developed region. This result can be explained from a physical standpoint: the thermal boundary-layer thickness is very thin and the temperature distribution in the core region is uniform in the region near the entrance $z = 0$, and the magnitude of the thermal dispersion effect is damped in the near wall region as shown in the region of $Y < 1$ in Fig. 8. So that the weak mixing of the local fluid stream in the thin boundary layer does not yield a significant transport of heat; however, the thickness of the thermal boundary layer increases with the increase of axial distance, then the strong mixing of fluid streams in the region of $Y > 1$ as shown in Fig. 8 makes the temperature gradient much smoother and enhances the heat transfer.

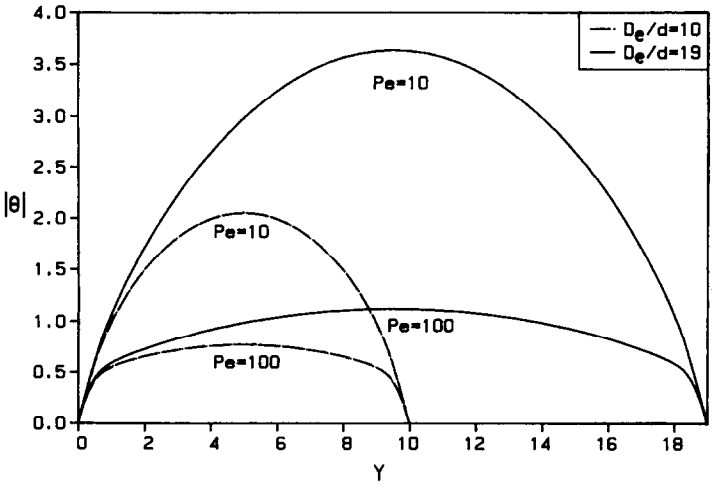

FIG. 9. Dimensionless temperature distribution along the symmetrical line $x = a/2$ for $K_P = \infty$, $Pe = 10$ and 100, and $D_e/d = 10$ and 19.

In many engineering applications, the thermal boundary conditions in forced convection cannot be considered either uniform wall temperature or uniform heat flux. It may be practical to know under what wall condition parameter the thermal boundary condition may be considered as circumferentially uniform heat flux or circumferentially uniform wall temperature for the forced convection in a horizontal square channel filled with packed spheres. It can be found from Fig. 11 that the differences between the values of Nu and $K_P = 0$ and 0.01 are less than 0.3%. Therefore, the thermal boundary condition with $K_P \leqslant 0.01$ may be considered as circumferentially uniform heat flux. Similarly, the curves of $K_P = 100$ and ∞ in Fig. 11 lie closer together, so that the thermal boundary condition with $K_P \geqslant 100$ may be considered as circumferentially uniform wall temperature. The values of K_P for cases 1 and 2 in the present experiment

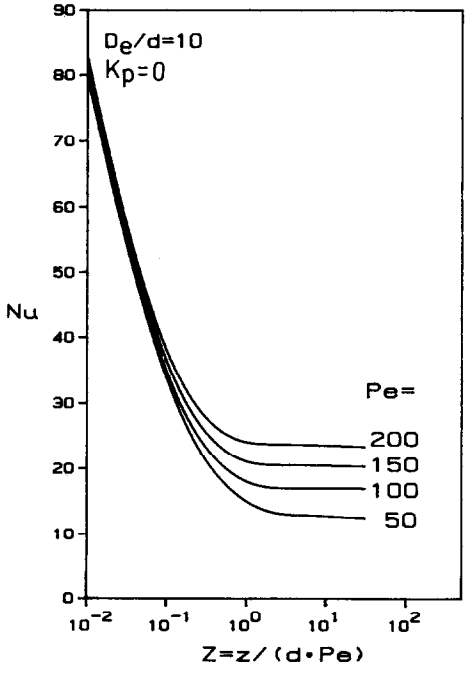

FIG. 10. Local Nusselt number vs dimensionless axial distance Z for $D_e/d = 10$, $K_P = 0$, and $Pe = 50$, 100, 150 and 200.

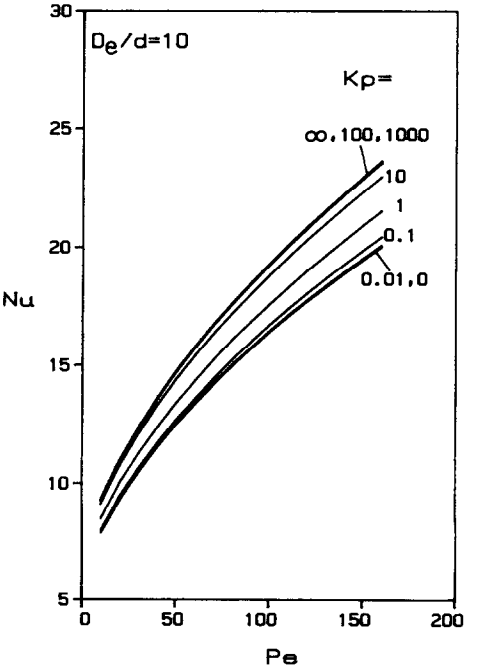

FIG. 11. Wall conduction effect on the Nusselt number variation for $D_e/d = 10$.

are about 10 and 60, respectively. Therefore, the variations of the Nusselt number for both the two limiting cases, $K_P = \infty$ and 0, are shown in Figs. 5 and 6.

5. CONCLUDING REMARKS

(1) A theoretical model is developed under the consideration of the effects of boundary, inertia, channelling and thermal dispersion to study the non-Darcian forced convection in the horizontal packed-sphere channels. The theoretical prediction of Nusselt number is in good agreement with the experimental data for two different channels: $4.75 \times 4.75 \times 85$ cm and $9.5 \times 9.5 \times 60$ cm.

(2) The values of fully-developed Nusselt number are influenced mainly by the channelling effect when the Peclet number is small, but the thermal dispersion effect becomes dominant when the Peclet number is high.

(3) Though the average velocity is the same under a fixed Pe, the velocity distribution is different in the channel for different D_c/d. The near wall velocity is higher in the channel with smaller D_c/d due to the relatively stronger channelling effect. Consequently, both the velocity and thermal dispersion effect in the core region are higher in the cases of larger D_c/d.

(4) Though the velocity in the core region for $D_c/d = 19$ is only slightly higher than that for $D_c/d = 10$, the high Peclet number, such as $Pe > 100$, magnifies the difference and induces significantly higher thermal dispersion conductivity. Thus the Nusselt number for $D_c/d = 19$ is higher than $D_c/d = 10$ even under a fixed Pe.

(5) The effect of thermal dispersion on heat transfer is rather weak in the near entrance region but eventually becomes significant in the thermally fully-developed region.

Acknowledgement—Financial support for this research provided by the National Science Council of Republic of China through Grant NSC 79-0401-E008-16 is greatly appreciated.

REFERENCES

1. K. Vafai and C. L. Tien, Boundary and inertia effects on flow and heat transfer in porous medium, *Int. J. Heat Mass Transfer* **24,** 195–203 (1981).
2. K. Vafai, Convective flow and heat transfer in variable porosity media, *J. Fluid Mech.* **147,** 233–259 (1984).
3. K. Vafai, R. L. Alkire and C. L. Tien, An experimental investigation of heat transfer in variable porosity media, *ASME J. Heat Transfer* **107,** 642–647 (1985).
4. M. Kaviany, Laminar flow through a porous channel bounded by isothermal parallel plates, *Int. J. Heat Mass Transfer* **28,** 815–858 (1985).
5. P. Cheng and C. T. Hsu, Fully-developed forced convective flow through an annular packed-sphere bed with wall effects, *Int. J. Heat Mass Transfer* **29,** 1843–1853 (1986).
6. P. Cheng and H. Zhu, Effect of radial thermal dispersion on fully-developed forced convection in cylindrical packed tubes, *Int. J. Heat Mass Transfer* **30,** 2373–2383 (1987).
7. P. Cheng and D. Vortmeyer, Transverse thermal dispersion and wall channelling in a packed bed with forced convective flow, *Chem. Engng Sci.* **43,** 2523–2532 (1988).
8. D. Poulikakos and K. J. Renken, Forced convection in a channel filled with porous medium, including the effects of flow inertia, variable porosity, and Brinkman friction, *ASME J. Heat Transfer* **109,** 880–888 (1987).
9. K. J. Renken and D. Poulikakos, Experiment and analysis of forced convection heat transport in a packed bed of spheres, *Int. J. Heat Mass Transfer* **31,** 1399–1408 (1988).
10. K. J. Renken and D. Poulikakos, Experiments on forced convection from a horizontal heated plate in a packed bed of glass spheres, *ASME J. Heat Transfer* **111,** 59–65 (1989).
11. M. L. Hunt and C. L. Tien, Non-Darcian convection in cylindrical packed beds, *ASME J. Heat Transfer* **110,** 378–384 (1988).
12. S. M. Kuo and C. L. Tien, Transverse dispersion in packed-sphere beds, *ASME Proc. 1988 Natn. Heat Transfer Conf.*, Houston, pp. 629–634 (1988).
13. C. Beckermann and R. Viskanta, Forced convection boundary layer flow and heat transfer along a flat plate embedded in a porous medium, *Int. J. Heat Mass Transfer* **30,** 1547–1551 (1987).
14. A. Nakayama, T. Kokudai and H. Koyama, Non-Darcian boundary layer flow and forced convective heat transfer over a flat plate in a fluid-saturated porous medium, *ASME J. Heat Transfer* **112,** 157–162 (1990).
15. F. C. Chou and W. Y. Lien, Forced convection in a parallel plate channel filled with packed spheres, *Proc. 1990 AIAA/ASME Thermophysics and Heat Transfer Conf.*, HTD-Vol. 139, pp. 57–64 (1990).
16. R. F. Benenati and C. B. Brosilow, Void fraction distribution in packed beds, *A.I.Ch.E. Jl* **8,** 359–361 (1962).
17. S. Ergun, Fluid flow through packed columns, *Chem. Engng Prog.* **48,** 89–94 (1952).
18. R. K. Shah and A. L. London, *Laminar Flow Forced Convection in Ducts*, p. 28. Academic Press, New York (1978).
19. D. Vortmeyer and J. Schuster, Evaluation of steady flow profiles in rectangular and circular packed beds by a variational method, *Chem. Engng Sci.* **38,** 1691–1699 (1983).

ANALYSE ET EXPERIENCE DE LA CONVECTION NON DARCYENNE DANS DES CANAUX CARRES A LIT FIXE DE SPHERES—1. CONVECTION FORCEE

Résumé—On présente une étude numérique et expérimentale de la convection forcée non Darcyenne dans des canaux carrés à lit fixe de sphères. Les résultats théoriques sont en accord avec les résultats expérimentaux. Les valeurs du nombre de NUSSELT pleinement établi sont principalement influencées par les cheminements préferentiels quand le nombre de PECLET est petit, mais la dispersion thermique devient dominante quand le nombre de PECLET est élevé. L'effet de la dispersion thermique sur le transfert de chaleur est plutôt faible dans la région proche de l'entrée, mais devient plus sensible dans la région thermiquement établie. Le rapport du diamètre hydraulique équivalent au diamètre de la sphère D_e/d affecte sensiblement le nombre de NUSSELT quand le nombre de PECLET est élévé; cela est encore principalement dù à l'effet de la dispersion thermique.

ANALYTISCHE UND EXPERIMENTELLE UNTERSUCHUNG DER NICHT-DARCY'SCHEN KONVEKTION IN EINEM MIT KUGELN GEFÜLLTEN, HORIZONTALEN QUADRATISCHEN KANAL—1. ERZWUNGENE KONVEKTION

Zusammenfassung—Die nicht-Darcy'sche erzwungene Konvektion in einem mit Kugeln gefüllten, horizontalen quadratischen Kanal wird numerisch und experimentell untersucht. Dabei zeigt sich gute Übereinstimmung. Der Wert der Nusselt-Zahl bei voll ausgebildeter Strömung wird hauptsächlich vom Kanalisierungseffekt bei kleinen Peclet-Zahlen beeinflußt, während bei großen Peclet-Zahlen der Einfluß der thermischen Dispersion überwiegt. Dieser Einfluß auf den Wärmetransport ist im Eintrittsbereich ziemlich schwach, wird aber im thermisch voll ausgebildeten Gebiet relativ bedeutsam. Das Verhältnis des gleichwertigen hydraulischen Durchmessers zum Kugeldurchmesser beeinflußt die Nusselt-Zahl bei großen Peclet-Zahlen entscheidend. Dies wird wieder hauptsächlich durch den Effekt der thermischen Dispersion verursacht.

АНАЛИЗ И ЭКСПЕРИМЕНТАЛЬНОЕ ИССЛЕДОВАНИЕ НЕ ПОДЧИНЯЮЩЕЙСЯ ЗАКОНУ ДАРСИ КОНВЕКЦИИ В ГОРИЗОНТАЛЬНЫХ КАНАЛАХ КВАДРАТНОГО СЕЧЕНИЯ С УПАКОВКАМИ СФЕР

Аннотация—Численно и экспериментально исследуется не подчиняющаяся закону Дарси вынужденная конвекция в горизонтальных каналах квадратного сечения с упаковками сфер. Найдено, что теоретические результаты согласуются с экспериментальными данными. При малых значениях числа Пекле значения числа Нуссельта полностью развитого течения преимущественно определяются каналовым эффектом, в то время как при больших значениях числа Пекле доминирующим становится эффект тепловой дисперсии. Влияние тепловой дисперсии на теплоперенос является достаточно слабым во входном участке, но усиливается в термически полностью развитой области. Отношение эквивалентного гидравлического диаметра к диаметру сферы D_e/d оказывает существенное влияние на зачение числа Нуссельта при высоких значениях числа Пекле, что тоже в основном обусловлено эффектом тепловой дисперсии.